International Journal of Signal Processing, Image Processing and Pattern Recognition
Vol.9, No.8 (2016), pp.329-342
http://dx.doi.org/10.14257/ijsip.2016.9.8.29

A Variational Framework for Image Super-Resolution and Its Applications

Todd Wittman[1]

[1]*Department of Mathematics, The Citadel, Charleston, SC, USA*
twittman@citadel.edu

Abstract

Image super-resolution is the process of combining multiple images into a single image that has higher resolution than any of the original images. We present a variational framework for fusing multiple co-registered images using the Total Variation (TV) and Mumford-Shah regularizations. We also propose an alternating minimization strategy for aligning and fusing multiple images in the case when the co-registration parameters are unknown. We discuss applications to video enhancement and present two novel applications to barcode scanning and Magnetic Resonance Imaging (MRI).

Keywords*: Image super-resolution, Image inpainting, Image registration, Total Variation, Mumford-Shah energy, Calculus of variations*

1. Introduction

It is very difficult to digitally zoom a single image to produce an image that has a significantly higher effective resolution than the original image. One way to break the "pixel limit" of an image is to combine multiple images of the same scene, such as a video sequence, into a single high-resolution image. This process is called *super-resolution.* Huang and Tsai were the first to notice that sub-pixel motion in an image sequence and image aliasing gave the potential for the construction of higher resolution images. The authors described two basic steps in the super-resolution process: image registration and data fusion [1].

Let $\{u_i: \Omega_i \to \Re\}_{1\le i\le N}$ denote the original sequence of N low-resolution grayscale images, where Ω_i denotes the lattice or grid of pixels of the i^{th} image. Let $M \ge 1$ denote the desired magnification factor. That is, we expect the final image to have M times as many pixels as the original image (s). The goal of super-resolution is to fuse the information of the entire image sequence to produce a single high-resolution image $u: \Omega_M \to \Re$, where Ω_M denotes the high-resolution lattice.

The first and often most difficult step of super-resolution is the registration step. We need to properly align the images u_i to a common grid Ω_M. Let $\varphi_i: \Omega_i \to \Omega_M$ denote the coordinate transformation mapping the image u_i to the high-resolution grid. Determining the transformations φ_i is often an ill-posed problem, so we generally restrict the class of allowable transformations. For example, if the visual scene is sufficient distance from the camera to ignore parallax effects, we could restrict φ_i to the class of planar homographies [2]. For this paper, we will restrict the camera/scene motion to translations. The methods we discuss could extend to general planar homographies, but as we consider more general transformations the problem becomes more difficult computationally.

There exist several methods for image registration under a translational model, notably the method by Irani and Peleg [3]. However, for a magnification factor $M > 1$ the registration needs to be precise to the sub-pixel level, often a very difficult if not insurmountable task. It is assumed that the transformation φ_i maps to the discrete gridpoints of Ω_M, so for a continuous warping it may be necessary to round the position of pixel $\varphi_i(x)$ to its nearest gridpoint on Ω_M. Once the images are aligned to a common

ISSN: 2005-4254 IJSIP
Copyright ⓒ 2016 SERSC

high-resolution lattice Ω_M, we obtain an image-like data set on Ω_M with some pixels having known value, some unknown, and some pixels having multiple values addressed to them (see Figure 1). Each pixel $x \in \Omega_M$ in the final image can be mapped backwards to a corresponding pixel $\varphi_i^{-1}(x)$ in each of the low-resolution images u_i. The corresponding gray value or color in the original low-resolution image will then be given by $u_i \circ \varphi_i^{-1}(x)$.

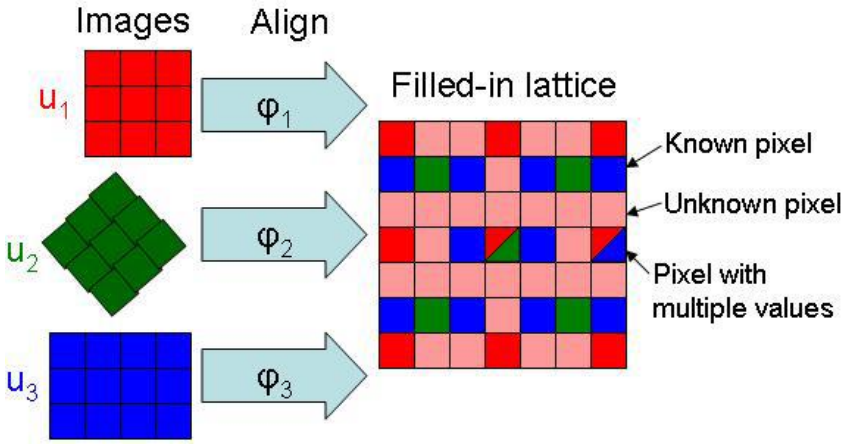

Figure 1. Illustration of the Image Registration Step

The second step of super-resolution is a fusion step that combines the registered images into a single high-resolution image u. The simplest image fusion approach is to take the median through all pixel values

$$u(x) = median\{u_i \circ \varphi_i^{-1}(x) \mid \varphi_i^{-1}(x) \in \Omega_i\}, \quad x \in \Omega_M.$$

The median image is commonly used as the benchmark for super-resolution algorithms. More sophisticated approaches use the Maximum Likelihood Estimate [3] and the Maximum A Posteriori model [4]. Some fusion algorithms are scene-aware, such as the method developed by Baker and Kanade for human faces [5]. In the next section, we will present a variational framework for data fusion.

2. Variational Super-Resolution

The variational approach to image processing is a general strategy that has proven effective for a wide variety of problems including denoising, deblurring, inpainting, and segmentation [6]. In simplest terms, the idea is to create an energy that describes the overall "quality" of an image and then optimize the energy to produce a superior image. For example, given a noisy grayscale image $f: \Omega \to \Re$ defined on some lattice Ω, we can compute a denoised image $u: \Omega \to \Re$ by minimizing the general energy.

$$\min_u E[u \mid f] = R(u) + \lambda \int_\Omega (u - f)^2 \, dx.$$

The first term $R(u)$ represents a regularization term describing the smoothness of the resulting image u. The second term of the energy is called the fidelity or matching term and forces the computed image to remain close to the original image in the least squares sense. The parameter λ is a weight chosen to control the balance between the regularization term and the fidelity term.

As mentioned previously, the super-resolution result relies heavily on precise determination of the registration functions φ_i. We will separately consider the cases when the coordinate transformations φ_i are known and unknown. Assuming the transformations

 Copyright ⓒ 2016 SERSC

φ_i are known will greatly simplify the problem by eliminating the registration step and will generally produce better final results. However, in general this is not a practical assumption for real-world applications.

2.1. Data Fusion with Known Registration

The variational model for image denoising extends naturally to multiple images. Instead of the fidelity term matching to a single image, the final image should match on average all images in the sequence in the least squares sense. Suppose we are given a sequence of N images $u_i: \Omega_i \to \Re$ and the corresponding registration functions $\varphi_i: \Omega_i \to \Omega_M$ that map the images to a common high-resolution lattice Ω_M. Each low-resolution image u_i will map pixel values to the registered image domain on the set $D_i := \Omega_M \cap \varphi_i(\Omega_i)$. The variational super-resolution model evolves a new image $u: \Omega_M \to \Re$ by minimizing the energy

$$\min_u E[u \mid u_{1\le i\le N},\ \varphi_{1\le i\le N}] = R(u) + \frac{\lambda}{N}\sum_{i=1}^{N}\int_{D_i}\left(u - u_i \circ \varphi_i^{-1}\right)^2 dx.$$

This model will perform variational smoothing on the known pixels and inpainting in unknown regions. However, the model is not equivalent to matching to the mean image, as pixels with multiple consistent values will receive more weight in the minimization.

There are many possible choices for the regularization energy $R(u)$ and it is often developed to perform a specific task. In this paper, we will focus on two of the most popular regularization strategies: the Total Variation (TV) norm [7] and the Mumford-Shah energy [8].

The TV regularization was first proposed in the seminal paper by Rudin, Osher, and Fatemi [7]:

$$R_{TV}(u) = \int_\Omega \|\nabla u\|\, dx.$$

TV regularization encourages image smoothness while allowing for the presence of jumps and discontinuities, a key feature in image processing because of the importance of edges in vision. The norm is generally chosen to be the L^2-norm

$$\|\nabla u\| = \sqrt{u_x^2 + u_y^2}.$$

There are several methods for minimizing the TV energy, including PDE-based methods [9], graph cuts [10], and Bregman iteration [11-12]. We performed TV minimization by modifying the digital TV filter proposed by Chan, Osher, and Shen [13]. We initialize the image $u^{(0)}$ as the median image and then evolve a new image $u^{(n)}$ for $n \ge 1$ according to the formulas

$$u^{(n+1)}(x) = \frac{\sum_{y\in N(x)} h^{(n)}(y)\, u^{(n)}(y) + \frac{\lambda}{N}\sum_{i=1}^{N} 1_{D_i}(x)\, u_i \circ \varphi_i^{-1}(x)}{\sum_{y\in N(x)} h^{(n)}(y) + \frac{\lambda}{N}\sum_{i=1}^{N} 1_{D_i}(x)}$$

$$h^{(n)}(y) = \frac{1}{\left\|\nabla u^{(n)}(y)\right\|}$$

where $N(x)$ is the 4-connected neighborhood of pixel x and $1_{D_i}(x)$ is the region indicator function

$$1_{D_i}(x) = \begin{cases} 1 & \text{if } x \in D_i \\ 0 & \text{otherwise} \end{cases}.$$

Copyright ⓒ 2016 SERSC

The gradient in the formula for $h^{(n)}$ can be approximated using a standard finite difference scheme. To avoid division by zero, a small lifting parameter $a > 0$ can be introduced into the norm

$$\frac{1}{\left\|\nabla u^{(n)}(y)\right\|} \approx \frac{1}{\sqrt{a^2 + \left\|\nabla u^{(n)}(y)\right\|^2}}.$$

The digital TV filter computation is stable for $a = O(10^{-4})$ [13].

Another popular choice for the regularization term $R(u)$ is the Mumford-Shah energy [8]. Suppose the image $u: \Omega_M \to \Re$ has a corresponding edge set Γ. The Mumford-Shah regularization is

$$R_{MS}(u, \Gamma) = \int_{\Omega_M \setminus \Gamma} \|\nabla u\|^2 dx + \gamma L(\Gamma)$$

where $L(\Gamma)$ is the one-dimensional Hausdorff measure indicating the length of the edge set and γ is a parameter determining the weight of the edge term. The first term smooths the image away from the edges and the second term minimizes the total edge length. Minimizing the Mumford-Shah energy is more difficult computationally than minimizing the TV energy, because it requires simultaneously tracking both u and Γ. The advantage of the Mumford-Shah energy is that it tends to give sharper edges and smoother flat regions. The resulting images are crisper but may also have a "cartoon-like" appearance.

There are several algorithms for minimizing the Mumford-Shah energy such as level sets [14] and graph cuts [15]. We implemented an alternating minimization scheme using the Ambrosio-Tortorelli Γ-convergence approximation to track the edge set [16]. Let $z: \Omega_M \to [0,1]$ denote the "edge canyon" function with $z = 0$ on the edge set and $z = 1$ otherwise. For a small parameter $\varepsilon > 0$, the Γ-convergence approximation to the Mumford-Shah regularization is given by

$$R_{MS}(u, z) = \int_{\Omega_M} z^2 \|\nabla u\|^2 dx + \gamma \int_{\Omega_M} \left(\varepsilon \|\nabla z\|^2 + \frac{(1-z)^2}{4\varepsilon} \right) dx.$$

The associated Euler-Lagrange equations are

$$-\nabla \cdot (z^2 \|\nabla u\|) + \frac{\lambda}{N} \sum_{i=1}^{N} 1_{D_i}(x) \left(u - u_i \circ \varphi_i^{-1} \right) = 0$$

$$\|\nabla u\|^2 z + \gamma \left(-2\varepsilon \Delta z + \frac{z-1}{2\varepsilon} \right) = 0.$$

We assume Neumann boundary conditions for the variables at the image boundaries

$$\frac{\partial u}{\partial \vec{n}} = \frac{\partial z}{\partial \vec{n}} = 0.$$

These equations can be solved by an elliptic solver such as Gauss-Jacobi, alternating the minimization of u and z. For inpainting problems, setting the parameter $\varepsilon = 1$ will usually suffice [17].

To produce artificial datasets with known registration functions, we aligned a high-resolution video sequence manually and then worked with downsampled versions of the data. Figure 2, shows the result of super-resolution of a 5-image sequence with magnification factor $M = 4$ and using the 3rd image of the sequence as the base image for alignment. The center image shows the result using the TV regularization with $\lambda = 20$. The image at right shows the result using Mumford-Shah regularization with $\lambda = 20$ and $\gamma = 2000$. Both super-resolution results are clearly superior to the original image. The

 Copyright ⓒ 2016 SERSC

super-resolution results are similar, but the Mumford-Shah regularization produces slightly sharper edges than the TV regularization.

Figure 2. Comparison of TV and Mumford-Shah Super-Resolution

The algorithm extends easily to color images by simply applying the process to each color channel. Figure 3, compares the super-resolution results to zooming a single image with different interpolation techniques: nearest neighbor, bilinear, bicubic, and staircased cubic. Clearly making use of the entire image sequence produces higher quality images. The Mumford-Shah super-resolution also outperforms simply taking the median of the image sequence.

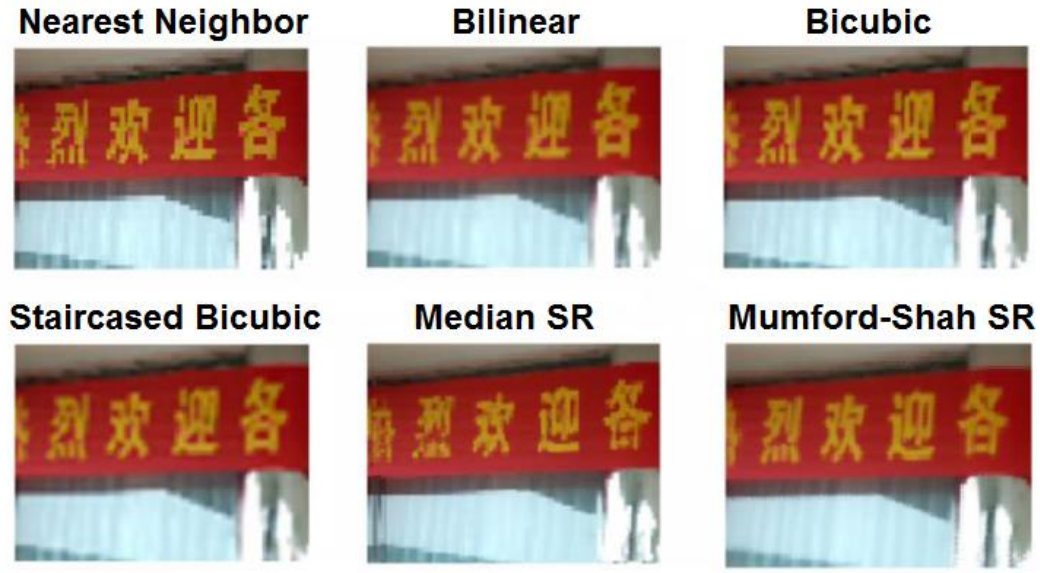

Figure 3. Zooming A Single Image Vs. Super-Resolution of an Image Sequence

The super-resolution procedure extends naturally to video processing. Each frame of the video is repeatedly selected as the base frame, aligning all other frames to the upsampled lattice of the base. Figure 4, shows video super-resolution of an 11-frame video sequence with known registration. The text is not legible in any of the orginal 11 frames, but becomes much clearer after super-resolution. The features of the woman's face are also improved, but the face appears somewhat unrealistic. Because it minimizes the edge length, the Mumford-Shah model is well-suited for lines and text, but tends to over-smooth textured regions. This suggests variational super-resolution is best suited for applications that do not require photo-realistic images.

Copyright ⓒ 2016 SERSC

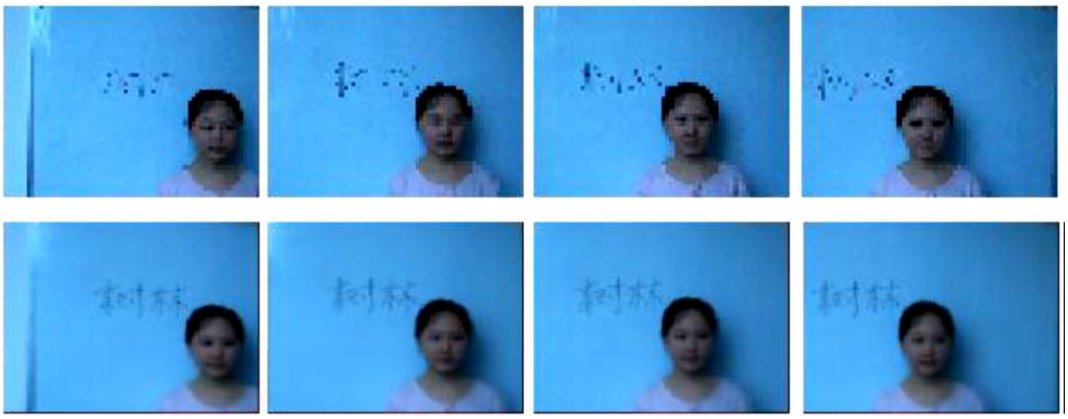

Figure 4. Mumford-Shah Super-Resolution of A Video Sequence

2.2. Simultaneous Registration and Fusion

In most applications, the registration functions φ_i will be unknown and the super-resolution problem becomes much harder. To make the problem tractable, the registration functions should be restricted to a suitable class of spatial transformations. For example, Irani and Peleg outline an iterative refinement based on a truncated Taylor series for affine transformations consisting of rotations, translation, and scaling [3]. We found that this iterative refinement worked well on low-resolution lattices, but the result was not accurate enough on the high-resolution lattice Ω_M to produce acceptable results. That is, the registration was accurate to the pixel level but not the sub-pixel level.

To refine the registration, we propose an alternating minimization model. Suppose one of the images in the sequence is identified as the base frame and the high-resolution lattice Ω_M is generated by upsampling this frame's lattice. Each low-resolution image is aligned to the low-resolution base frame and the aligned images are upsampled to the lattice Ω_M. The minimum energy image u is computed from this registration, followed by minimizing over the registration functions for this image. The process continues, alternately freezing and minimizing the image and registration functions until the registration functions reach a steady-state.

Note that if the initial registration is accurate to the pixel level on the low-resolution lattice, then this registration will be accurate within $\left\lfloor \frac{M}{2} \right\rfloor$ pixels on the high-resolution lattice. For rigid transformations, the update to the registration functions can be computed by a local search of pixel mappings on Ω_M. We implemented this procedure using the Mumford-Shah model and restricting the transformations to simple translations

$$\varphi_i(x, y) = (x + a, y + b) \uparrow M$$

where $\uparrow M$ denotes upsampling by a factor M. The initial registration was computed by the Irani-Peleg method and the updates were computed by a local enumerative search over the window within $\left\lfloor \frac{M}{2} \right\rfloor$ units of the (a, b) translation parameters.

For most sequences, the process converged within three iterations and resulted in a better image than using the initial registration. However, if the initial registration was not accurate enough, the resulting image was poor. This is because the alternating minimization is drawn towards a local minimum close to the initialization which may not correspond to the global minimum over u and φ jointly. The alternating minimization helps refine the registration, but the initial registration still needs to be precise.

Figure 5, compares the super-resolution result with known registration to the super-resolution result with the alternating minimization method. Both images are clearly an improvement over the original image, but the second image is less blurred than the third.

 Copyright ⓒ 2016 SERSC

However, the second image was produced synthetically using known registration parameters. The third image is based only on the input video sequence and is reproducible in practice.

Figure 5. Super-Resolution with Known and Unknown Registration Functions

3. Applications of Super-Resolution

3.1. Video Enhancement

The variational method we outlined can be used to enhance certain types of video. One application is to enhance traffic surveillance video for vehicle tracking and recognition. Figure 6, shows one frame of a video sequence taken from a stationary camera over an intersection in Karlsruhe, Germany. Performing super-resolution on the original video would accomplish little, as the streets would be blurred by moving vehicles and the stationary objects do not exhibit sub-pixel shifts to permit enhanced resolution. On the other hand, tracking a moving vehicle would be a good candidate for super-resolution. The camera is far enough from the scene that parallax effects are negligible as long as the vehicle does not change direction. The four vehicles indicated in Figure 6, were tracked manually for 11 consecutive frames.

Figure 6. Frame from Traffic Video of Intersection in Karlsruhe

Each of the four vehicle sequences were enhanced by a magnification factor $M = 4$ using the Mumford-Shah alternating minimization method with $\lambda = 5$ and $\gamma = 2000$. The

registration assumes a translational model. As Figure 7, shows, the super-resolution result gives a clearer picture of the vehicle than just using bicubic interpolation to zoom a single frame.

However, the images appear to be blurred with a horizontal jitter effect. It is likely that the video was interlaced: the odd and even lines were acquired separately and the vehicle changed position slightly during the acquisition phase. To de-interlace the video, each frame is separated into two images consisting of alternating horizontal lines. This new set consisting of twice the number of frames is then sent through the same super-resolution algorithm. To maintain the aspect ratio of the original frame, a blank row is inserted on alternating lines for the inpainting mask. The de-interlaced images are crisper and features such as windows and tires are more visible on the vehicles.

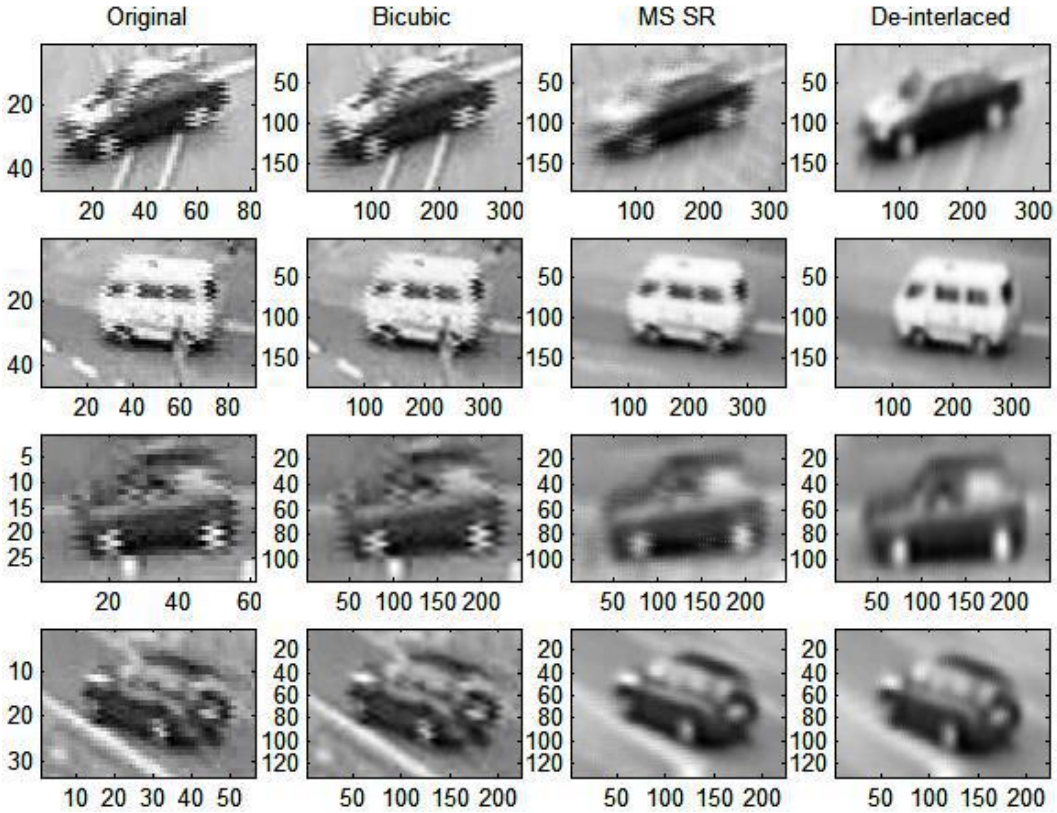

Figure 7. Super-Resolution of Four 11-Frame Sections of Video in Figure 6

3.2. Barcode Scanning

A linear barcode is a series of alternating black and white stripes encoding information in the relative widths of the bars. The traditional barcode scanners are laser scanners that extract a 1D signal from the barcode. Imaging scanners that obtain a full 2D image of the barcode are also being used more in practice, especially as cellphones become more common. However, the imaging scanners generally have much lower resolution than the laser scanners, resulting in poorer decoding performance for image-based systems. Many barcodes that would be decoded by a traditional laser scanner cannot be decoded by a modern imaging scanner.

The current imaging software treats each row of the image as a separate scanline and attempts to decode it. If we think of each of the barcode scanlines as a separate one pixel high image, super-resolution can be used to create a single high-resolution signal from the collection of scanlines. Even though we are only working with a single image, we are

 Copyright ⓒ 2016 SERSC

using the super-resolution concept to fuse multiple pieces of information into a single high-resolution result.

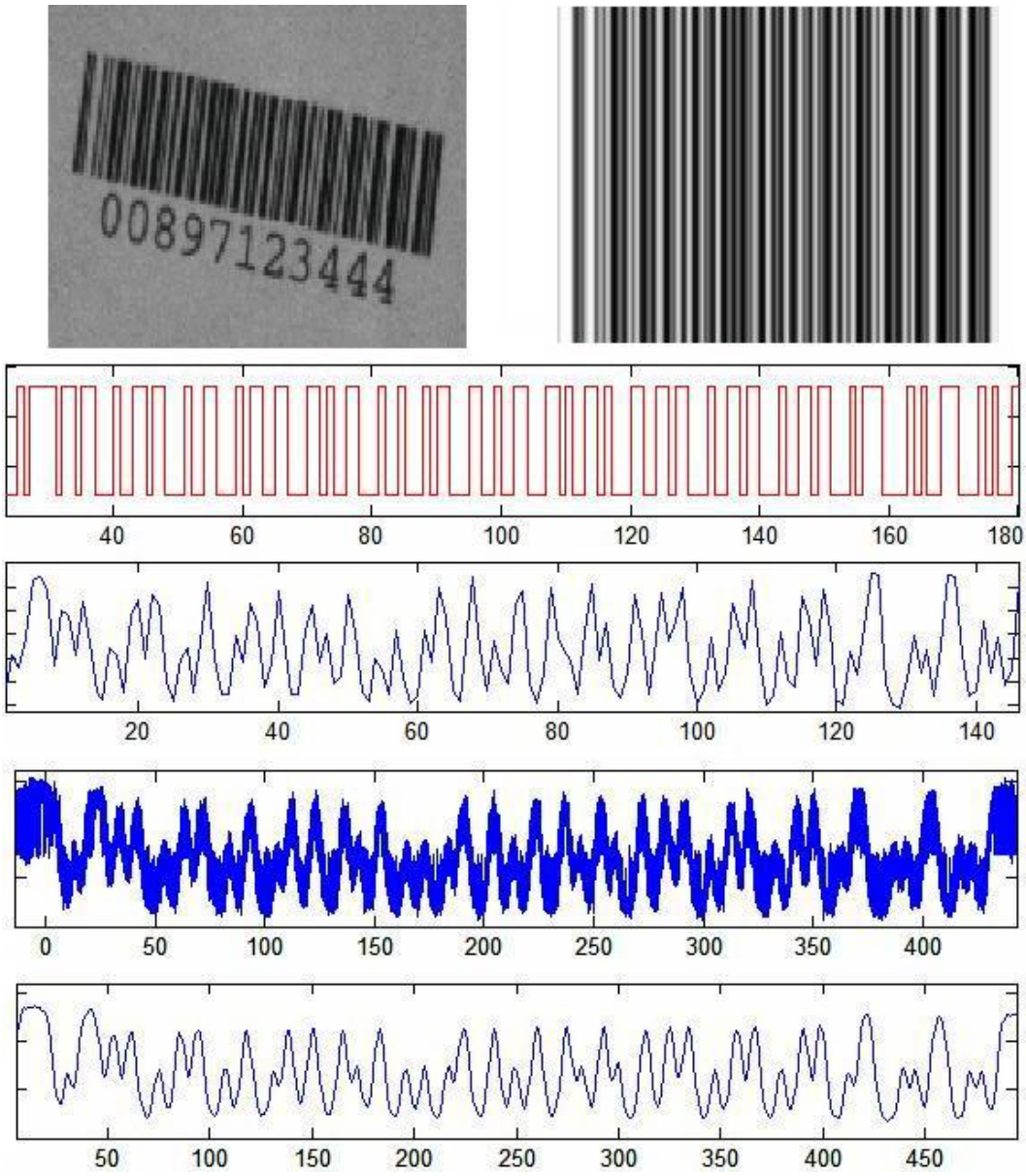

Figure 8. TV Super-Resolution of Code 128A Barcode Image

Figure 8, shows a Code 128A barcode image that would not decode using traditional software. The first signal plotted is the ideal signal for this barcode. The second signal is a scanline taken from the center of the image, which has length 150 pixels. The third plot shows the result when we project all scanlines in the image to a common axis. Note this signal is very noisy and consists of many more data points. The TV regularization has been shown to be effective for denoising 1D barcode signals, as it tends to produce blocky signals [18-19]. We applied the TV super-resolution method with $\lambda = 10$. The resulting signal is shown in the bottom row of Figure 8. Although it appears similar visually to the original signal, this signal has higher resolution than the original signal and gives more accurate information about the location of the peaks and valleys, so it is decoded correctly by the barcode software.

Copyright ⓒ 2016 SERSC

The super-resolution process allows us to potentially decode barcodes that would not have been decoded otherwise. As an experiment, we ran the TV super-resolution algorithm on a library of 71 barcode images that were misdecoded by decoding software. A misdecode is a case where the scanner incorrectly interpreted the signal as the wrong information, whereas a non-decode occurs when the scanner failed to interpret the barcode as any information. Since barcodes are used for tracking sensitive items such as airplane parts and medication, obtaining a non-decode result is highly preferable to a misdecode. The same decoding software was able to correctly decode 28 (39%) of the super-resolved barcodes. Even more encouraging, all of the remaining 43 barcodes were detected as a non-decode rather than a misdecode. However, the computational costs of aligning the datasets make it difficult to implement this procedure in a real-time system.

3.3. Reconstruction from MRI Sensor Data

In a phased-array Magentic Resonce Imaging (MRI) apparatus, multiple independent receiver elements (coils) are placed around the subject, generally at equally spaced intervals along a circle or ellipse. Each of the sensors obtains a graycale image $u_i: \Omega_i \rightarrow \Re$ that is accurate close to the sensor, but quickly goes dark and becomes noisy far from the sensor position, as shown in Figure 9. Each sensor has a sensitivity profile $P_i: \Omega_i \rightarrow \Re$ that reflects the sensitivity or confidence of the i^{th} sensor at each pixel. In theory, each sensor image u_i is derived from the ideal total image u by multiplying by the sensitivity profile with additive Gaussian noise n_i:

$$u_i(x) = P_i(x)u(x) + n_i(x).$$

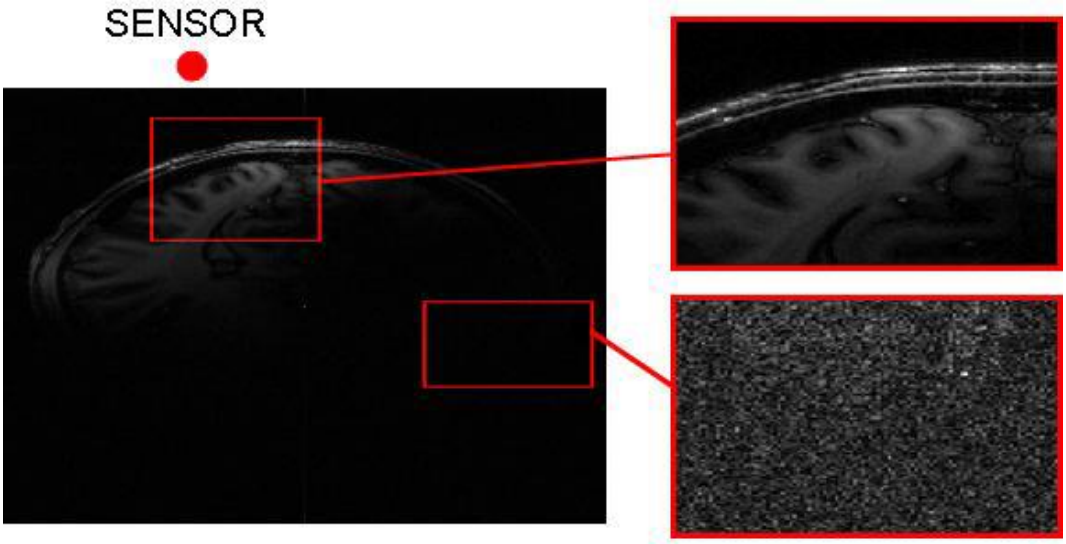

Figure 9. Image from A Single MRI Sensor

The standard approach for combining a set of N sensor images is to take the L^2-norm through the images

$$v(x) = \sqrt{\sum_{i=1}^{N} |u_i(x)|^2}.$$

It has been shown that among all known reconstruction techniques without knowledge of the sensitivity profiles, the L^2-norm produces images with the highest SNR [20]. However, the resulting image tends to be very dark in the center, as seen in the center

 Copyright ⓒ 2016 SERSC

image in Figure 10. Generally, contrast enhancement techniques are required to view the image.

It is possible to incorporate the sensitivity profiles P_i into our super-resolution model by making a small adjustment to the matching term:

$$\min_u E[u \mid u_{1\le i\le N},\ \varphi_{1\le i\le N}] = R(u) + \frac{\lambda}{N}\sum_{i=1}^{N}\int_{D_i}\left(P_i u - u_i \circ \varphi_i^{-1}\right)^2 dx.$$

However, this requires knowledge of the sensitivity profile P_i for each sensor. Since magnetic force decays with the square of the distance from the source, we propose the sensitivity profile

$$P_i(x) = \exp\left(-\frac{d^2(x, s_i)}{\sigma^2}\right)$$

where s_i is the position of the i^{th} sensor and σ is a parameter indicating the rate of decay. The sensor position s_i may be directly measured on the MRI apparatus. If this information is not available, we can interpolate the sensor positions by tracing backwards from the L^2-norm image $v(x)$ to the sensor images u_i. Matching $P_i v$ and u_i in the least squares sense gives the sensor positions s_i and sensitivity parameter σ by

$$\min_{s_i,\sigma}\sum_{i=1}^{N}\left(\exp\left(-\frac{d^2(x, s_i)}{\sigma}\right)v(x) - u_i(x)\right)^2.$$

Figure 10, shows an example of interpolating sensor positions from sensor images.

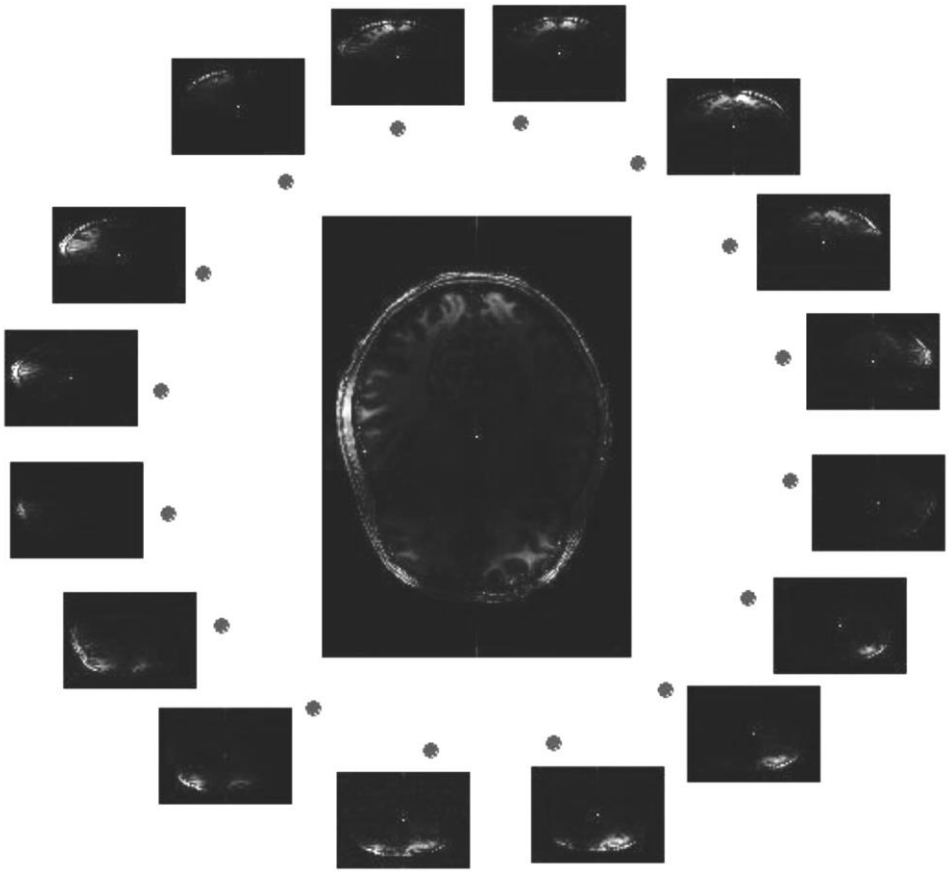

Figure 10. Positions of 16 MRI Sensors Found by Backwards Tracing

Copyright ⓒ 2016 SERSC

Figure 11, shows the result of Mumford-Shah super-resolution with $\lambda = 100$ and $\gamma = 2000$. We used the interpolated sensor positions shown in Figure 10. The L^2-norm image is bright around the edges but dark in the center, a well-known problem in MR image processing. The super-resolved image is brighter and the contrast is more consistent throughout the image. Also, many of the noise and texture features have been smoothed. This may or may not be a desirable feature for medical analysis, as diagnosis depends on shape but also texture.

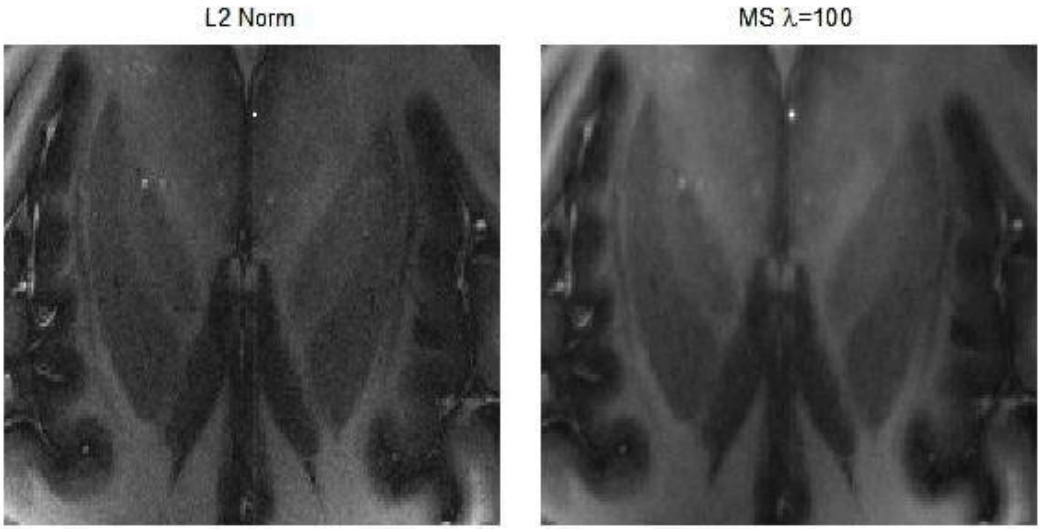

Figure 11. Comparison of L2 Image and Super-Resolution Image

4. Conclusions and Further Research

We have presented a variational framework for image super-resolution that can handle the cases when the registration functions are known and unknown. We focused on the TV and Mumford-Shah energies, but there are other regularization strategies that may be suited for specific purposes. It is possible to incorporate a blur kernel into the model to help sharpen the resulting image. It is also possible to consider non-local features to interpolate textures and produce more photo-realistic results.

We have also presented applications of super-resolution beyond the standard application of video processing. Super-resolution is the process of fusing multiple datasets together and should not be narrowly interpreted. We have shown that the variational super-resolution model can improve barcode scanning and MRI analysis in certain situations. It may be possible to extend the super-resolution concept to other interesting applications, such as audio processing and hyperspectral images.

Acknowledgments

The author would like to thank Dr. Shulin Yang, Dr. Fadil Santosa, Dr. Steen Moeller, Prof. Jackie Shen, and Dr. Miroslav Trajkovic for their invaluable help and support on this project.

References

[1] T. Huang and R. Tsai, "Multi-frame Image Restoration and Registration", Adv. Computer Vision and Image Processing, vol. 1, **(1984)**, pp. 317-339.
[2] D. Capel and A. Zisserman, "Computer Vision Applied to Super Resolution", IEEE Signal Processing Magazine, **(2003)**.
[3] M. Irani and S. Peleg, "Improving Resolution by Image Registration", Graphical Models and Image Processing, vol. 53, **(1991)**, pp. 231-239.

 Copyright ⓒ 2016 SERSC

[4] R. Schultz and R. Stevenson, "Extraction of High-resolution Frames from Video Sequences", IEEE Trans. Image Processing, vol. 5, **(1996)**, pp. 996-1011.
[5] S. Baker and T. Kanade, "Limits on Super-resolution and How to Break Them", IEEE Trans. Pattern Analysis and Machine Intelligence, vol. 24, **(2002)**, pp. 1167-1183.
[6] T. Chan and J. Shen, "Image Processing and Analysis: Variational, PDE, Wavelet, and Stochastic Methods", SIAM Press, Philadelphia, **(2005)**.
[7] L. Rudin, S. Osher and E. Fatemi, "Nonlinear Total Variation Based Noise Removal Algorithms", Physica D, vol. 60, **(1992)**, pp. 259-268.
[8] D. Mumford and J. Shah, "Optimal Approximations by Piecewise Smooth Functions and Associated Variational Problems", Comm. Pure and Applied Math., vol. 42, **(1989)**, pp. 577-685.
[9] A. Chambolle, "An Algorithm for Total Variation Minimization and Applications", Journal of Mathematical Imaging and Vision, vol. 20, **(2004)**, pp. 89-97.
[10] Y. Boykov, O. Veksler and R. Zabih, "Fast Approximate Energy Minimization vis Graph Cuts", IEEE Trans. Pattern Analysis and Machine Intelligence, vol. 23, **(2001)**, pp. 1222-1239.
[11] T. Goldstein and S. Osher, "The Split Bregman Method for L1 Regularized Problems", SIAM Journal on Imaging Science, vol. 2, no. 2, **(2009)**, pp. 323-343.
[12] S. Osher, M. Burger, D. Goldfarb, J. Xu and W. Yin, "An Iterative Regularization Method for Total Variation Restoration", Multiscale Modeling and Simulation, vol. 4, no. 2, **(2005)**, pp. 460-489.
[13] T. Chan, S. Osher and J. Shen, "The Digital TV Filter and Nonlinear Denoising", IEEE Trans. Image Processing, vol. 10, **(2001)**, pp. 231-241.
[14] T. Chan and L. Vese, "A Level Set Algorithm for Minimizing the Mumford-Shah Functional in Image Processing", Proceedings of 1st IEEE Workshop on Variational and Level Set Methods in Computer Vision, Vancouver, Canada, **(2001)**, July 13.
[15] E. Bae and X. Tai, "Efficient Global Optimization for the Multiphase Chan-Vese Model of Image Segmentation by Graph Cuts", Proceedings of 7th International Conference of Energy Minimization Methods in Computer Vision, Bonn, Germany, **(2009)**, August 24-27.
[16] L. Ambrosio and V. Tortorelli, "Approximation of Functionals Depending on Jumps by Elliptic Functionals via Γ-convergence", Comm. Pure and Applied Math., vol. 43, **(1990)**, pp. 999-1036.
[17] S. Esedoglu and J. Shen, "Digital Inpainting Based on the Mumford-Shah-Euler Image Model", European Journal Applied Math., vol. 13, **(2002)**, pp. 353-370.
[18] S. Esedoglu, "Blind Deconvolution of Barcode Signals", Inverse Problems, vol. 20, **(2004)**, pp. 121-135.
[19] T. Wittman, "Lost in the Supermarket: Decoding Blurry Barcodes", SIAM News, vol. 37, **(2004)**.
[20] E. Larsson, D. Erdogmus, R. Yan, J. Principe and J. Fitzsimmons, "SNR Optimality of Sum-of-squares Reconstruction for Phased-array Magnetic Resonance Imaging", Journal of Magnetic Resonance, vol. 163, **(2003)**, pp. 121-123.

Author

Todd Wittman is an assistant professor of mathematics at The Citadel in Charleston, SC. He received the PhD in Applied Mathematics in 2006 from University of Minnesota. He did his postdoctoral research at UCLA under the supervision of Prof. Andrea Bertozzi and Prof. Stanley Osher. His research interests include PDEs, optimization, the calculus of variations, and their applications to problems in image processing.

Copyright ⓒ 2016 SERSC

Copyright ⓒ 2016 SERSC